Projection of future fire emissions over the contiguous US using explainable artificial intelligence and CMIP6 models

Sally S.-C. Wang[1], L Ruby Leung[1], and Yun Qian[1]

[1]Atmospheric Sciences and Global Change Division, Pacific Northwest National Laboratory

February 1, 2023

Abstract

Increasing temperature and water cycle changes due to warming climate may increase wildfire activities. Reliable projections of fire emissions are critical for informing fire management to address fire impacts on societies and ecosystems. Here, we construct a neural network (NN) model explained by the Shapley Additive explanation (SHAP) to predict fire $PM_{2.5}$ emissions change and understand their drivers over the contiguous US (CONUS) in the mid-21st century under a high greenhouse gas emissions scenario (SSP5-8.5). Using future meteorology and leaf area index (LAI) simulated by eight global climate models from the Coupled Model Intercomparison Project Phase 6 (CMIP6), future population density, and present-day land use and land cover (LULC) as input to the NN model, the total fire $PM_{2.5}$ emissions over CONUS are projected to increase by 4-75% (model spread). Among different regions, fire emissions in the western US are projected to increase more significantly in June-July-August (JJA) than in other seasons and regions, with the median ratios of future to present-day fire emissions ranging from 1.67 to 2.86. The increases in fire emissions are mainly driven by increasing normalized temperature (23-29%) and decreasing soil moisture (2-10%) in the future. When future LULC change is considered, the projected fire emissions further increase by 58%-83% over the western US compared to projections without LULC change because of future increases in vegetation fraction. The results highlight the important role of warmer temperature, decreasing soil moisture, and LULC change in increasing fire emissions in the future.

Projection of future fire emissions over the contiguous US using explainable artificial intelligence and CMIP6 models

Sally S.-C. Wang[1], L. Ruby Leung[1], and Yun Qian[1]

[1] Atmospheric Sciences and Global Change Division, Pacific Northwest National Laboratory, Richland, Washington, USA

Corresponding author: Sally S.-C. Wang (sing-chun.wang@pnnl.gov) and L. Ruby Leung (Ruby.Leung@pnnl.gov)

Key Points:

- Using explainable AI and CMIP6 outputs, total fire $PM_{2.5}$ emissions over the US are projected to increase by 4-75% by mid-century.
- Fire emissions will increase by 67-186% in the western US in summer, due to reduced soil moisture and warmer temperature in the future.
- Land use and land cover change adds an extra ~50% increase of future fire emissions, driven by increased vegetation in the western US.

Abstract

Increasing temperature and water cycle changes due to warming climate may increase wildfire activities. Reliable projections of fire emissions are critical for informing fire management to address fire impacts on societies and ecosystems. Here, we construct a neural network (NN) model explained by the Shapley Additive explanation (SHAP) to predict fire $PM_{2.5}$ emissions change and understand their drivers over the contiguous US (CONUS) in the mid-21st century under a high greenhouse gas emissions scenario (SSP5-8.5). Using future meteorology and leaf area index (LAI) simulated by eight global climate models from the Coupled Model Intercomparison Project Phase 6 (CMIP6), future population density, and present-day land use and land cover (LULC) as input to the NN model, the total fire $PM_{2.5}$ emissions over CONUS are projected to increase by 4-75% (model spread). Among different regions, fire emissions in the western US are projected to increase more significantly in June-July-August (JJA) than in other seasons and regions, with the median ratios of future to present-day fire emissions ranging from 1.67 to 2.86. The increases in fire emissions are mainly driven by increasing normalized temperature (23-29%) and decreasing soil moisture (2-10%) in the future. When future LULC change is considered, the projected fire emissions further increase by 58%-83% over the western US compared to projections without LULC change because of future increases in vegetation fraction. The results highlight the important role of warmer temperature, decreasing soil moisture, and LULC change in increasing fire emissions in the future.

Plain Language Summary

Climate change has increased fire frequency and size in the United States, particularly in the western US, causing property damage, threats to human life, and degraded air quality. Frequent drought, enhanced fuel aridity, and increased fuel accumulation may cause larger and more frequent fires and emissions in the coming decades. Using explainable artificial intelligence (XAI) and outputs from global climate models, we show that total fire $PM_{2.5}$ emissions over the contiguous US will be around 1.38 times the present-day emissions by the mid-21st century under a high greenhouse gas emissions scenario. The fire $PM_{2.5}$ emissions will double in the western US during summer, mainly driven by drying trends in the soil along with increasing temperatures. When the future change of land use and land cover is also considered, the fire emissions in the western US will increase further by 50%, due to the increased vegetation fractions in a warmer climate.

1 Introduction

Wildfires have become larger and more frequent across the United States over the past two decades, with more notable changes in the western US. Several studies have suggested that the increased wildfire burned areas are driven by increased fuel aridity, warming temperature, and fuel management (Abatzoglou & Williams, 2016; Burke et al., 2021; Marlon et al., 2012; Westerling et al., 2006). With the increased fire activities in the recent five years, the burned area has increased by ~3 times and costs in fire suppression have increased by ~8 times in the recent decades compared to the 1980s (NIFC, 2022). The fires emitted large amounts of fine particulates with a diameter of 2.5 μm or less ($PM_{2.5}$), leading to degraded air quality and increased exposure to smoke from fires (Jaffe et al., 2020; Kaulfus et al., 2017; Liu et al., 2018; O'Dell et al., 2019). Understanding how fire emissions will change under future climate and the key factors controlling the changes in future fire emissions is important for fire management and planning to reduce the impacts on human health and air quality in the coming decades.

Several studies have projected increased fire emissions over the contiguous US (CONUS) in the future, mainly the western US, using different approaches (Ford et al., 2018; Liu et al., 2021; Neumann et al., 2021; Val Martin et al., 2015; Xie et al., 2022; Yue et al., 2013; Table 1). One commonly used approach is the process-based fire model embedded in the Dynamic Global Vegetation Model (DGVM), which uses empirical functions of fire activity and climate, vegetation, and socioeconomic variables to estimate burned area and fire emissions (Pechony & Shindell, 2009; Thonicke et al., 2010). For example, Ford et al. (2018) projected 54% and 50% increases in organic carbon (OC) and black carbon (BC) over CONUS in mid-century under the Representative Concentration Pathway (RCP) 8.5 scenario, using a process-based fire model implemented in Community Land Model (CLM) driven by meteorological fields simulated by Community Earth System Model (CESM). Using the Sixth Coupled Model Intercomparison Project (CMIP6) multimodel and multiensemble simulations, Xie et al. (2022) projected 130-260% increases in fire CO_2 emissions over the western US under the Shared Socioeconomic Pathways (SSP) 5-8.5 scenario in late 21st century. In addition to DGVM, another widely used approach is the statistical regression model, which is based on the statistical relationship between fires and the associated predictors to predict burned area and fire emissions. Yue et al. (2013) used regression and parameterization driven by climate simulations and projected increases of 80-170% in OC and BC over the western US in the mid-21st century. Recently, Liu et al. (2021) used an empirical fire model with DGVM and projected 50% increases in fire $PM_{2.5}$ emissions over the western US in the mid-21st century, considering the changes in both climate and fuel.

The approaches mentioned above have their strengths and weaknesses. Process-based fire models with DGVMs can simulate the non-linear relationships between fires and predictors and capture the feedback among climate, vegetation, and fires. However, they often assume the same relationships across the globe or regions and apply universal functions or the same set of parameters to all the grid cells in a model (Pechony & Shindell, 2009; Thonicke et al., 2010). In addition, process-based models with DGVMs are more computationally expensive than regression models, which are computationally efficient and can achieve promising performance. However, the good performance of regression models is limited by the assumption of linear relationships between fires and predictors, which work well at large spatial scales (e.g., ecoregions) but may not be applicable for projecting fire changes considering the non-linear relationships among multiple factors at finer spatial scales. Combining the advantages of the two approaches, machine learning (ML) provides a solution to model the non-linear relationships between fires and predictors at fine spatial scales efficiently. Prior studies have used various ML approaches to predict fire occurrence, burned area, and fire emissions at different temporal and spatial scales (Birch et al., 2015; Coffield et al., 2019; Cortez & Morais, 2007; Dillon et al., 2011; Kane et al., 2015; Wang et al., 2021; Wang & Wang, 2020). Recently, to fill the gaps of interpretability of ML, explainable artificial intelligence (XAI) has been developed and applied to understand the relationships learned by the ML and identify the key contributing predictors (Adadi & Berrada, 2018; Arrieta et al., 2020).

Here, we leverage the power of XAI and the atmospheric forcing and vegetation from the CMIP6 multimodel simulations to project fire emissions over CONUS in the mid-21st century (2050-2065) under the SSP5-8.5 scenario. We first construct an artificial neural network (ANN) to predict monthly fire $PM_{2.5}$ emissions using predictors of local and large-scale meteorology, land surface characteristics, and population density from observations and reanalysis data. We then evaluate the performance of the ANN model driven by the historical simulations of eight global climate models (GCMs) and identify the GCM biases that influence the fire emissions predicted by the ANN model. Two experiments are conducted for future projection. For the first experiment, future fire emissions are projected by driving the ANN model with the future climate projections and LAI from the eight GCMs, future population density, and present-day land use and land cover (LULC) from satellite observations. For the second experiment, we select four of the eight GCMs that provide future LULC outputs and drive the ANN with future climate projection, LAI, population density, vegetation distributions, and LULC. We compare the future projections with and without LULC change for the same four GCMs to isolate the effects of LULC change on future fire emissions.

Table 1. Prior studies projecting future fire emissions over CONUS

Fire model	Region	Scenario	Period	# GCMs	Projected changes	Note	Ref
Regression	WUS, 1980-2004	CMIP3 A1B scenario	2046-2065	15	increase~80 % for OC and BC	Climate factor only; assume fuel consumption remains constant	Yue et al. (2013)
Parameterization					~170% and 150% increase for OC and BC		
DVGM (CESM fully coupled)	WUS,2000	RCP 4.5	2050	1	60% increase for OC	Online computed meteorology and prescribed sea-surface and sea-ice distributions	Val Martin et al. (2015)
		RCP 8.5			decrease of 0.3% for OC		
DVGM (CLM)	CONUS, 2001-2010	RCP4.5	2040-2050	1	~125% increase for OC and BC	Future simulations were driven by meteorology from archived CESM1 simulation	Ford et al. (2018)
			2090-2100				
		RCP8.5	2040-2050		54% and 50% increase for OC and BC		
			2090-2100		150% and 141% increase for OC and BC		
Statistical model from Prestemon et al. (2016)	SEUS, 1992-2010	Scenario A2	2011-2060	1	13-62% **lower** for PM 2.5	They include climate and socioeconomic variables	Shankar et al. (2018)
Statistical model (empirical) and DGVM	WUS, 2001-2010	CMIP5 RCP 8.5 (meteorology for number/burned area) +	2050-2059	1	50% increase for PM2.5	They used two climate datasets (with different scenarios) for projection	Liu et al. (2021)

		CMIP3 SRES-A2 (fuel loading and moisture)					
Regression (from Yue et al. (2013))	WUS, 1996-2005	RCP 4.5	2046-2055	5	Average 8% increase for OC and BC (GISS-E2-R; small)	Climate factor only	Neumann et al. (2021)
		RCP 8.5	2086-2095		Average 17% increase for BC and OC (GISS-E2-R; small)		
DVGM (fully-coupled)	WUS, 2000-2014	CMIP6 SSP1-2.6	2080-2100	3	60-110% increase for CO_2 (Aug-Sep)		Xie et al. (2022)
		CMIP6 SSP2-4.5			100-150% increase for CO_2 (Aug-Sep)		
		CMIP6 SSP5-8.5			130-260% increase for CO_2		

2 Data

2.1 Fire-induced $PM_{2.5}$ emission data

Monthly fire $PM_{2.5}$ emission data for training and evaluating XAI is obtained from the Global Fire Emissions Database (GFED) version 4, with a spatial resolution of 0.25º available from 1997 to present. GFED obtains burned area from MODIS (MCD64A1) and provides fire $PM_{2.5}$ emissions estimated by the burned area, the emission factors from Akagi et al. (2011), and the fuel loads and combustion completeness from the Carnegie-Ames-Stanford Approach (CASA) biogeochemical model (van der Werf et al., 2017). In this study, the GFED fire $PM_{2.5}$ emission is the predictand of the neural network model. To match the spatial resolutions of the CMIP6 models, we regrid the fire emissions to 1º × 1º by area-weighted averaging. The target grid is computed as a weighted mean of all the grids from the source grids that intersect with the target grid and the weighting factor is the area of the intersection with each of the source grids.

2.2 Predictor data from observations and reanalysis for model training

We develop a neural network at 1º × 1º grid resolution driven by predictor variables at a monthly scale from 2000 to 2020. The predictor variables are regridded to 1º × 1º by area-weighted averaging. Table 2 shows the predictors in the model with their sources and original spatial and temporal resolutions. Compared to the variables used in Wang et al. (2022), this study used a subset of the variables that are accessible in the CMIP6 outputs.

Table 2. Predictor variables used in the NN model

Variables	Abbreviation	Categories	Temporal resolution	Spatial resolution	Data Source	References
Monthly mean relative humidity	RH	Local meteorology	monthly	32 km	North American Reanalysis (NARR)	Mesinger et al. (2006)
Monthly mean of daily precipitation	apcp	Local meteorology	monthly	32 km	North American Reanalysis (NARR)	Mesinger et al. (2006)
Monthly mean wind speed	wndsp	Local meteorology	monthly	32 km	North American Reanalysis (NARR)	Mesinger et al. (2006)
Monthly Standardized Precipitation Evapotranspiration Index	SPEI	Local meteorology	monthly	0.5º×0.5º	SPEI	Vicente-Serrano et al. (2010)
Monthly mean vapor pressure deficit	VPD	Local meteorology	daily	4 km	gridMET	Abatzoglou (2013)
Monthly normalized meteorology (normalized temperature, RH, apcp, and VPD)	Nor.temp, nor.rhum, nor.apcp, nor.VPD	Local meteorology	monthly	32 km/ 4 km	North American Reanalysis (NARR) /gridMET	Mesinger et al. (2006); Abatzoglou (2013)
Monthly standard deviation of daily SVDs for northern California	SVD1_NCA and SVD2_NCA	Large-scale meteorological patterns	monthly	Regional	North American Reanalysis (NARR)	Wang et al. (2021)
Monthly standard deviation of daily SVDs for southern Rocky Mountain	SVD1_SRM and SVD2_SRM	Large-scale meteorological patterns	monthly	Regional	North American Reanalysis (NARR)	Wang et al. (2021)
Monthly standard deviation of daily SVDs for southeastern US (with 2-month lag)	SVD1_SElag2 and SVD2_SElag2	Large-scale meteorological patterns	monthly	Regional	North American Reanalysis (NARR)	Wang et al. (2021)
Monthly mean surface soil moisture	soilm	Land-surface properties	monthly	0.25º×0.25º	Global Land Data Assimilation System (GLDAS-2)	Xia et al. (2012)
Monthly mean vegetation fraction	Veg_frac	Land-surface properties	monthly	0.25º×0.25º	Global Land Data Assimilation System (GLDAS-2)	Xia et al. (2012)

Monthly mean Leaf Area Index	LAI	Land-surface properties	8 days	500 m	MODerate resolution Imaging Spectroradiometer (MODIS); LAI classification scheme	Myneni et al. (2015)
Land cover fraction	Grass, tree, shrub, crop, nonveg, resid	Land-surface properties	Yearly	0.05º×0.05º	MODerate resolution Imaging Spectroradiometer (MODIS); LAI classification scheme	Friedl (2015)
Population density	Pop	Socioeconomic and coordinate variables	Yearly	30 arc	Gridded Population of the World data collection (GPW v4)	CIESIN-Columbia University (2017)

2.2.1 Local meteorology

Local meteorology includes monthly mean relative humidity (RH) at 2m, total precipitation, and wind speed at 10 m from the North American Regional Reanalysis (NARR (Mesinger et al., 2006) and vapor pressure deficit (VPD) from the gridMET dataset (Abatzoglou & Kolden, 2013). As drought dries the fuels and facilitates fire development, we also include the monthly Standardized Precipitation Evapotranspiration Index (SPEI) (Vicente-Serrano et al., 2010), which measures the drought severity based on climatic data as predictors.

To provide more information on the temporal variability of meteorology, we also include normalized meteorology, which is calculated by subtracting the long-term mean from 2000 to 2020 and dividing it by the standard deviation. We include the normalized monthly mean surface temperature, relative humidity (RH) at 2m, total precipitation, and VPD.

2.2.2 Large-scale meteorological patterns

Large-scale meteorological patterns influence wildfire occurrence and intensity by modulating local meteorological conditions (Crimmins, 2006; L. Dong et al., 2021; Trouet et al., 2009; Zhong et al., 2020). Wang et al. (2021) showed that including predictors of large-scale meteorological patterns associated with wildfires improves burned area prediction over CONUS. Therefore, we include predictors representing the synoptic patterns driving fire emission variability, constructed using the singular value decomposition (SVD) method (Wang et al., 2022). The leading nodes of SVDs were identified for the three regions where large fires periodically occur, including northern California, southern Rocky Mountains, and the southeastern US, as defined in Wang et al. (2021). For each region, we calculate the daily mean fire $PM_{2.5}$ emissions over the region and compute the day-to-day correlations between the regional mean fire $PM_{2.5}$ emissions and the five gridded daily meteorological variables (surface temperature, 2-meter RH, U-wind and V-wind at surface, and geopotential height at 500 hPa from NARR) for all $1^{o} \times 1^{o}$ grid cells within the large-scale domain, resulting in a correlation map for each meteorological variable. The correlation maps are then used to derive the SVD modes representing the large-scale meteorological patterns related to daily fire emissions. Finally, we compute the monthly standard deviation of the daily SVD time series for the first two SVD modes, representing the month-to-month variations of synoptic fluctuations and atmospheric instability. Note that we use U- and V-wind at the surface rather than at 850 hPa used in Wang et al. (2022) due to data availability in the CMIP6 archive. The detailed methods and discussions about the SVDs are provided in Wang et al. (2021) and Wang et al. (2022).

2.2.3 Land-surface properties and socioeconomic variables

We include predictors of monthly mean surface soil moisture, leaf area index (LAI), and vegetation fraction from the North American Land Data Assimilation System (NLDAS-2) to capture the effects of fuel availability and flammability (Xia et al., 2012). Land cover fraction of the LAI classification scheme is obtained from the Terra and Aqua combined MODIS Land Cover Climate Modeling Grid (CMG) Version 6 data (Friedl & Sulla-Menashe, 2015). The LAI classification scheme has 12 land types, including savannas, evergreen and deciduous broadleaf forest, evergreen and deciduous needleleaf forest, grass, shrub, broadleaf crop, non-vegetated land, urban, water bodies, and unclassified land. To match the land cover types in CMIP6, we combine savannas, evergreen and deciduous broadleaf forests as well as evergreen and deciduous needleleaf forests in the MODIS data to one type, corresponding to the "tree" in the GCMs; we also combine urban, unclassified, and water bodies to a single type, corresponding to "residual". The grass, shrub, broadleaf crop, and non-vegetated lands correspond to the grass, shrub, crop, and bare soil in the GCMs. This results in six different land cover types matching the land types defined in CMIP6, including tree, grass, shrub, crop, bare soil, and residual. Note that the MODIS land cover data starts from 2001, so we use the data of 2001 for 2000.

Population density is included to represent human effects on wildfires. The population density data is obtained from the Gridded Population of the World (GPW) data collection for the years 2000, 2010, 2015, and 2020, with a spatial resolution of 30 arc-second (CIESIN-Columbia University, 2017). The populations in other years are linearly interpolated between the four years.

2.3 CMIP6 model data

We use the monthly output from the eight selected GCMs in the CMIP6 archive, including the Australian Community Climate and Earth System Simulator Earth System Model Version 1.5 (ACCESS-ESM 1.5), Community Earth System Model Version 2 (CESM2), Euro-Mediterranean Centre on Climate Change couped climate model standard configuration (CMCC-CM2-SR5), EC-Earth3 coupled Climate-Carbon Cycle (EC-Earth-CC), EC-Earth3 coupled with the second-generation dynamic global vegetation model LPJ-GUESS (EC-Earth-Veg), EC-Earth-Veg with lower resolution (EC-Earth-VegLR), Geophysical Fluid Dynamics Laboratory Earth System Model Version 4.1 (GFDL-ESM 4.1), and the Canadian Earth System Model version 5 (CanESM 5) (Eyring et al., 2016; O'Neill et al., 2016). Model outputs include monthly mean RH, surface wind speed, total precipitation, LAI, and surface soil moisture. SPEI and VPD are computed based on monthly meteorology from CMIP6 data. SVDs are calculated from daily surface temperature, 2-meter RH, U-wind and V-wind at the surface, and geopotential height at 500 hPa. The CMIP6 model outputs are all regridded to $1^{o} \times 1^{o}$ by area-weighted averaging. Outputs from historical simulations and SSP5-8.5 future scenario from variant r1i1p1f1 are used for the present-day (2000-2014) simulation and future (2050-2065) projection. The SSP5-8.5 projects CO_2 emissions increasing strongly until 2080 and then slightly declining until the end of the century, with a radiative forcing peaking at 8.5 W/m^2 and a global mean temperature increase of around 4°C by 2100 compared to the current era (Eyring et al., 2016; IPCC, 2022). The future population density data is obtained from the Global One-Eighth Degree Population Base Year and Projection Grids Based on the Shared Socioeconomic Pathways for 2010-2100, with a spatial resolution of 0.125° (Jones & O'Neill, 2020). We use the projected population density under the SSP5 scenario.

As mentioned before, this study includes two projection experiments with four simulations, as shown in Table 3. The first experiment (land_fix) compares simulations 2 and 1, representing the impacts of future changes in meteorology, LAI, and population density on future fire emissions. The second experiment (land change) compares simulations 4 and 3, considering the effects of changes in meteorology, LAI, population density, as well as LULC on future fire emissions. The four GCMs are GFDL-ESM4, EC-Earth3-Veg, EC-Earth3-VegLR, EC-Earth-CC, which provide future natural vegetation and land use distribution (Döscher et al., 2022; Dunne et al., 2020; Hurtt et al., 2020; Lawrence et al., 2019; Song et al., 2021; Swart et al., 2019; Ziehn et al., 2020). Accordingly, we use the outputs of vegetation distribution and LULC from the four GCMs to project future fire emissions considering the effects of LULC change. The outputs of vegetation distribution and LULC include monthly vegetation fraction and yearly land cover fraction (tree, crop, grass, shrub, bare soil, and residual). Hereafter CMIP6 refers to the CMIP6 models used in this study.

Table 3. Experiments and simulations with the sources and states of the variables used in this study

Experiment	Simulation number	Meteorology and LAI	Population density	LULC
1. Land_fix (using eight GCMs)	1	GCM present-day	GPW present-day	MODIS present-day
	2	GCM future	GPW future	MODIS present-day
2. Land_change (using four GCMs)	3	GCM present-day	GPW present-day	GCM present-day
	4	GCM future	GPW future	GCM future

3 Method

3.1 Artificial neural Network (ANN)

ANN or neural network (NN) consists of several layers with interconnected neurons. The layers include input layer, hidden layer, and output layer. Each neuron in the input layer represents one predictor (e.g., monthly RH, surface soil moisture etc.) and the neuron in the output layer is the target which is fire $PM_{2.5}$ emission (g $m^{-2}month^{-1}$). During the training process, each neuron takes the weighted average from other neurons in the previous layer and transforms the average by the nonlinear activation functions. The weights are randomly initialized for all the neurons at the beginning of the training process. The same process applies to the neurons in the next layer until the output layer is reached and the errors between the final output and the target are measured using a loss function. Then the error is backpropagated from the last layer to the front layer to calculate the contributions of the weights and update the weights to minimize the errors between the final output and target using an optimization algorithm.

In this study, we construct an NN model with five layers, including one input layers with 25 neurons corresponding to the 25 predictors, three hidden layers with 200, 150, and 80 neurons, and one output layer corresponding to the predicted fire emission. The input variables are normalized using min-max normalization; that is, we subtract the minimum value of the predictor from each predictor value and divide the result by the difference between the maximum and minimum value, resulting in values ranging between -1 to 1. The formula can be presented as: $x' = \frac{x - \min(x)}{\max(x) - \min(x)}$, where x is the original value and x' is the normalized value. The optimization algorithm is stochastic gradient descent (SGD), the learning rate is 0.01, and the batch size is 64. The loss function is the mean square error (MSE), and the activation function is the Rectified Linear Unit (ReLU).

3.2 Model evaluation

To evaluate the model, we apply the 10-fold cross validation (CV) technique. The whole dataset during 2000-2020 is randomly separated into ten equal-size splits. For each round of CV, the model is trained with nine splits of the data and the trained model is then used to predict burned area in the remaining one split. The final evaluation is based on root mean square error (RMSE). Besides RMSE, we also use the correlation coefficient and the index of agreement (IoA) between the observed and predicted fire emissions to evaluate our model performance. The formula of IoA can be expressed as:

$$\mathrm{IoA} = 1 - \frac{\sum_{i=1}^{N}(y_i - \hat{y}_i)^2}{\sum_{i=1}^{N}(|\hat{y}_i - \bar{y}| + |y_i - \bar{y}|)^2}$$

where y_i is the observations, $\hat{y}_i$ is prediction, and $\bar{y}$ is the mean of the observations. The value of IoA ranges between 0 and 1, with values closer to 1 indicating a better fit.

3.3 Shapley Additive explanation (SHAP)

SHAP is an innovative approach that uses game theory to explain variable importance globally (i.e., the whole dataset) and locally (i.e., one sample) (Lundberg & Lee, 2017). Under the scope of SHAP, the predictors are the “players” in a co-operative game in which the goal is a prediction for a single target. Each predictor has its “playout” representing its contribution to the prediction, considering all possible combinations of the predictors. To calculate the predictor contribution for predictor i, the SHAP value considers the differences in the model's predictions f_x made by including and excluding the predictor i for all the combinations of predictors:

$$\phi_i = \sum_{S \subseteq F \setminus \{i\}} \frac{|S|!\,(F - |S| - 1)!}{F!} [f_x(S \cup \{i\}) - f_x(S)]$$

where ϕ_i is the weighted average of all marginal contribution of predictor i, F is the total number of features, S is the subset of predictors from all predictors except for predictor i, $\frac{|S|!(F-|S|-1)!}{F!}$ is the weighting factor counting the number of permutations of the subset S. $f_x(S)$ is the expected output given the predictors subset S. $[f_x(S \cup \{i\}) - f_x(S)]$ is the difference made by predictor i.

SHAP has been widely used to explain different machine learning models in many fields (Padarian et al., 2020; Stirnberg et al., 2021; Wang et al., 2021). It has been applied to deep neural network ("Deep SHAP") based on DeepLIFT method in Lundberg and Lee (2017), which approximates the conditional expectations of SHAP values using a selection of background samples.

4 Results

4.1 NN performance and variable importance

Figure 1 shows the maps of the observed and predicted fire emissions averaged over 2000–2020. The model reproduces the spatial patterns of fire emissions and captures the large fire emissions over northern California. The spatial correlation between the observed and predicted fire emissions is 0.79, showing a good agreement between the long-term observations and predictions. Additionally, the model can capture the interannual variability over CONUS, with a correlation of 0.94 and RMSE of 4.84 g/m^2. To assess model performance in different regions, Figures S1a-d show the time series of observed and predicted fire $PM_{2.5}$ emissions averaged over the selected regions. The selected regions include the western forest region (WFR), Mediterranean southern California (SCA), southwestern US (SWUS), and southeastern US (SEUS) (color boxes in Figure 1b). These regions frequently burn and share similar fire regimes and vegetation types. The predicted interannual variability resembles the observed interannual variability for the selected regions (IoA=0.31-0.95). However, the southwestern and southeastern US have much smaller IoA and larger RMSE than the other two regions in the western US (Table 4). The model has larger biases over the regions with much lower fire emissions (e.g., southeastern US) because the NN is dominated by grid cells that have large fire emissions (i.e., western US) (Zhu et al., 2022).

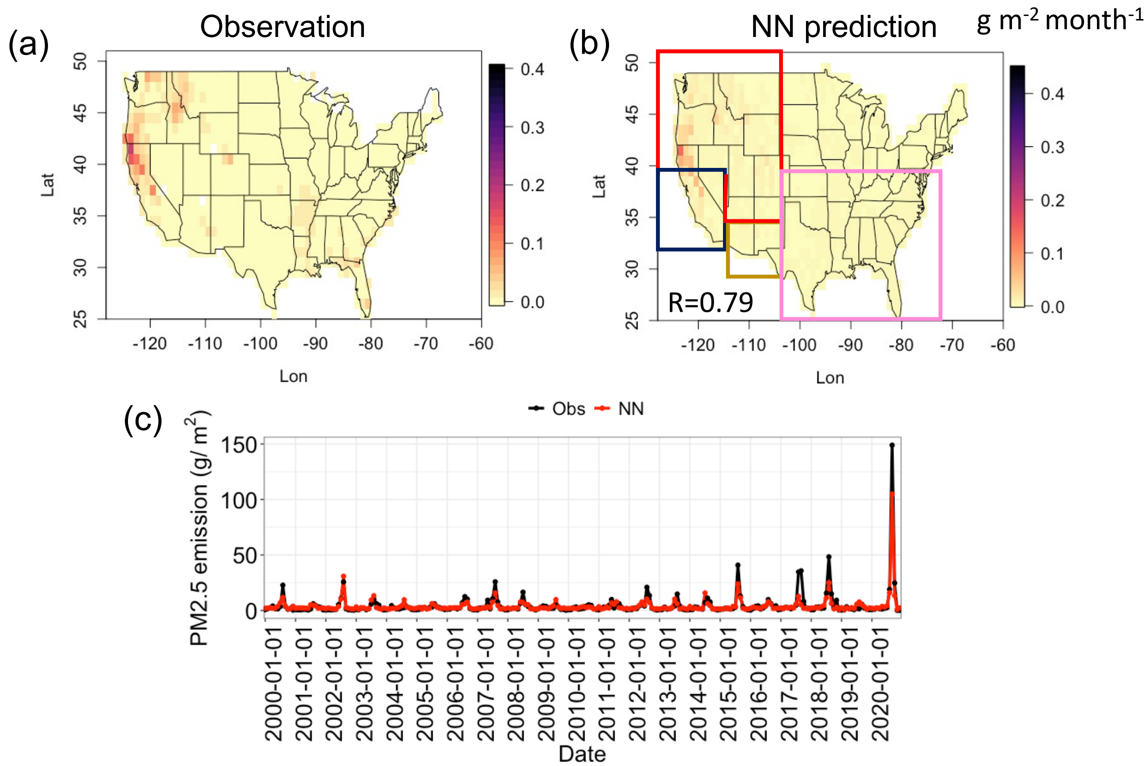

Fig. 1. The burned area map averaged over 2000 to 2020 for (a) observation and (b) prediction; (c) Time series of observed (black) and predicted (red) monthly fire $PM_{2.5}$ emissions averaged across CONUS. The color boxes in (b) denote four analysis regions: western forest area (WFR, red), Mediterranean southern California (SCA, blue), southwestern US (SWUS, dusty), and southeastern US (SEUS, pink).

Table 4. Model performance aggregated over the regions, including the western forest region (WFR), southern California (SCA), southwestern US (SWUS), and the southeastern US (SEUS).

	CONUS	WFR	SCA	SWUS	SEUS
IoA	0.94	0.88	0.95	0.31	0.44
RMSE (g m^{-2})	4.84	5.02	0.73	0.37	0.94

To understand the leading variables in the NN model at different time scales, we analyze the absolute SHAP values at seasonal and interannual scales by averaging the SHAP values of all the grids over CONUS for each year and month and take the absolute values. Predictors with larger |SHAP| have greater contribution and therefore, more important to fire emission. Figure 2 shows the mean |SHAP| values at seasonal and interannual time scales for CONUS. At both time scales, local meteorology and land-surface variables are critical, as most of them are included in the top 10 variables. Specifically, normalized temperature, normalized RH, RH, SVD2_sElag2, and soil moisture are the predominant variables controlling both interannual and seasonal variability of the fire emissions. Land-surface variables (LAI, vegetation fraction, and grass fraction) and VPD have larger contributions to fire emissions at the seasonal scale, as they have strong seasonality. Some variables, including SVD1_NCA, SVD1_SElag2, and SPEI, are more important at the interannual time scale.

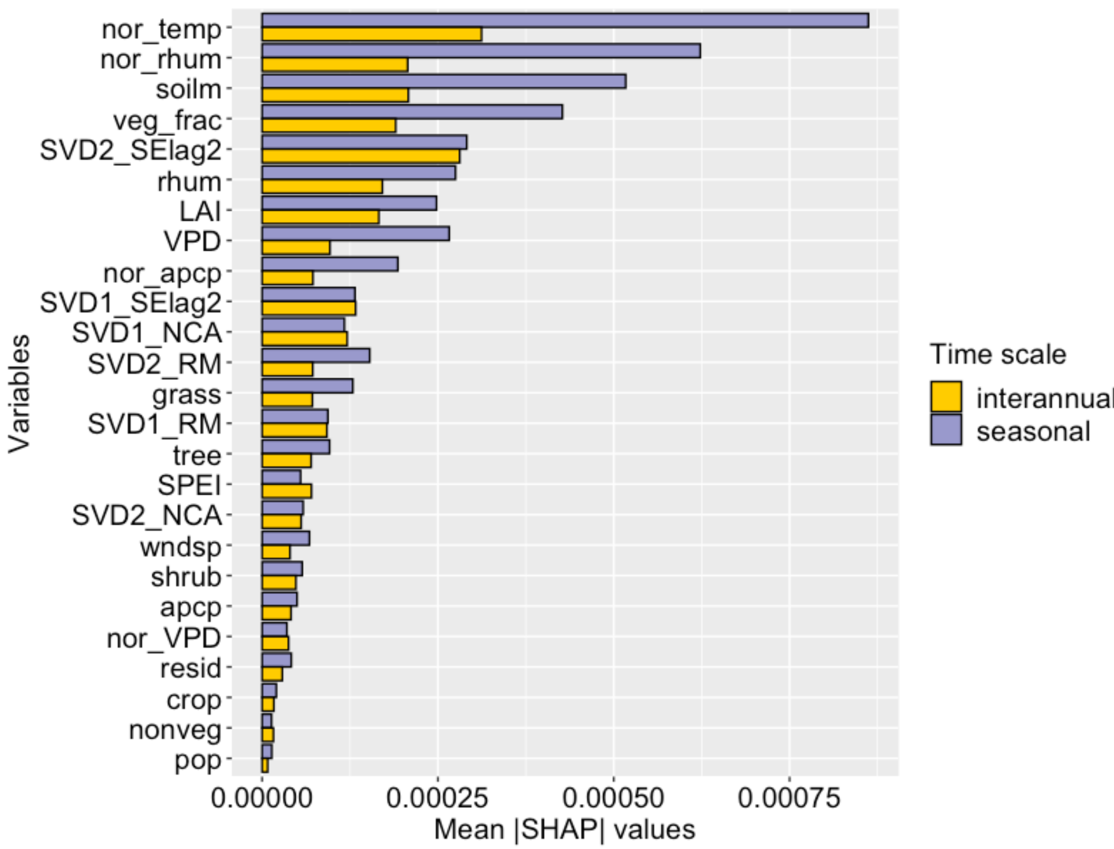

Fig. 2. Variable importance represented by the mean |SHAP| values at seasonal and interannual time scale.

4.2 GCM-NN present-day performance

Before utilizing the NN and GCM outputs to project future fire emissions, it is helpful to evaluate the prediction of present-day fire emissions by the NN with GCM meteorology and LAI, GPW population density, and MODIS land cover from 2000 to 2014 as predictors. The NN driven by GCM outputs is referred to as GCM-NN. Figure 3 shows the ratios of predicted to observed total fire emissions for CONUS and the four regions for the eight GCMs. The GCM-NN reproduces the present-day fire emissions well for CONUS, with a median ratio of 1.27. Focusing on the four regions where fires frequently occur, GCM-NN slightly overestimates fire emissions over southwestern US and southeastern US where the median values of the ratios are

1.18 and 1.12, respectively. The fire emissions over the western forest region are underestimated by the GCM-NN (Table 5 and Figure 3). To better understand the model performance, we also evaluate the seasonal variability and spatial distributions of the GCM-NN predicted fire emissions. Figure 4 shows the seasonal distribution of the observed and predicted fire emissions driven by the observation and reanalysis meteorology (red line in Figure 4) and GCM meteorology (purple line in Figure 4). The GCM-NN predictions generally reproduce the observed seasonality of fire emissions and capture the peak in August. Although the seasonality is well reproduced, the predicted spatial distributions of GCM-NN are inconsistent with the GFED fire emissions (Figure 5). For instance, the NN predictions driven by ACCESS, CESM, and CMCC outputs are overestimated over the Central Great Plains (Figures 5c-e). The NN driven by the outputs of CanESM and EC models overestimates fire emissions in the western forest region, mainly over the Rocky Mountains (Utah, Colorado, and Wyoming), and the NN with GFDL outputs overestimates fire emissions over the southeastern US (Figures 5f-j).

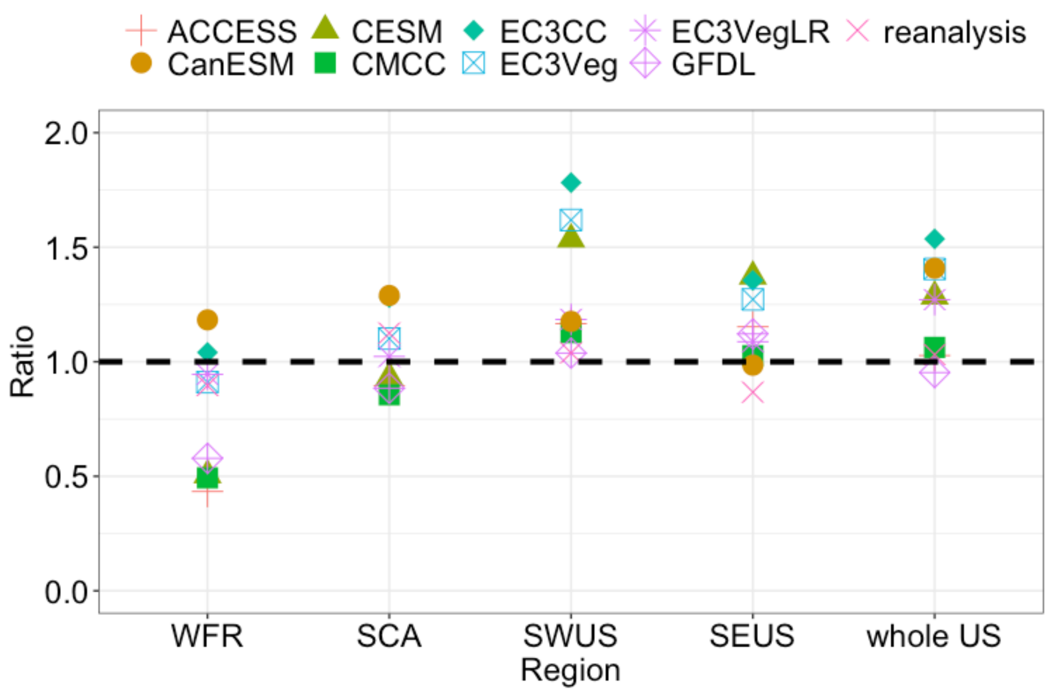

Fig. 3. Ratio of the GCM-NN predicted to the GFED observed fire PM2.5 emissions over CONUS and the four selected regions.

Table 5. Observations (mean of GFED fire emissions) and multi-model projections of fire emissions (Gg yr^{-1}) (median values of the 8 GCMs; 1Gg = 10^9 g). The regions include western forest region (WFR), southern California (SCA), southwestern US (SWUS), and southeastern US (SEUS).

	Observed (2000-2014)	Present-day (2000-2014) NN model	Future (2050-2065) NN model
WFR	0.082 ± 1.006	0.061 ± 0.292	0.099 ± 0.336
SCA	0.051 ± 0.571	0.050 ± 0.097	0.070 ± 0.153
SWUS	0.029 ± 0.682	0.034 ± 0.063	0.069 ± 0.171
SEUS	0.044 ± 0.266	0.050 ± 0.245	0.055 ± 0.204
CONUS	0.041 ± 0.550	0.052 ± 0.266	0.062 ± 0.215

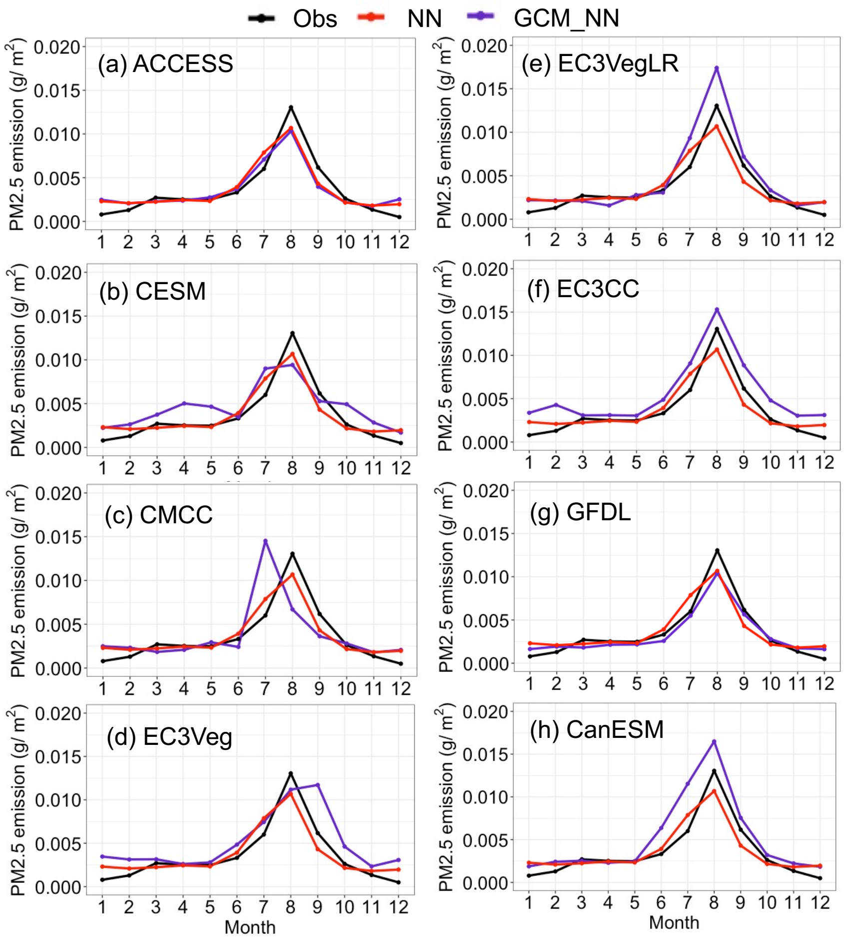

Fig. 4. Seasonal cycle of the averaged fire $PM_{2.5}$ emission from GFED (black line), the NN model driven by reanalysis (red line), and the GCM-NN models (purple lines). The fire $PM_{2.5}$ emissions are averaged over CONUS during 2000-2014 by month.

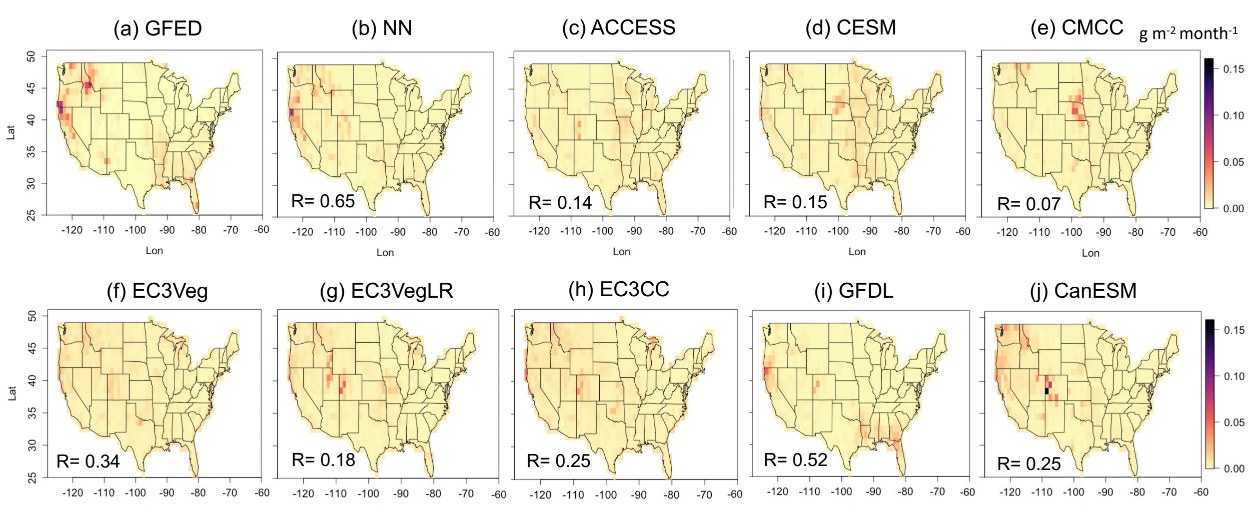

Fig. 5. Spatial distributions of the mean fire $PM_{2.5}$ emissions (g m^{-2} $month^{-1}$) averaged over 2000-

2014 from (a) GFED) and the NN model driven by observations (b) and different GCMs (c-j).

The inconsistency of the spatial patterns between GCM-NN and observations is dominated by the spatial biases in summer (June-August), which is the peak season of fire emissions (Figure S2). The spatial biases of the GCM-NN predicted fire emissions in summer may be contributed by biases of the NN model, biases of the GCM outputs used as predictors for the model, and interactions between these biases. To determine the relative contributions of the NN model biases (reanalysis-NN minus GFED) and the GCM predictor biases (GCM outputs minus reanalysis/observation), linear regression models are fitted to the model biases (GCM-NN minus GFED) in June-July-August (JJA) for different regions using NN biases and predictor biases at each grid point within the regions as predictors. Figure S3 shows the coefficient of the predictors for each GCM and region and only the predictors with $p<0.05$ are shown. Predictors with larger coefficients have larger contributions to the GCM-NN biases. For ACCESS, CESM, and CMCC, the positive biases in the Central Great Plains are mainly contributed by the NN biases (Figure S3e). The overestimations in the western forest region are due to biases in precipitation for CanESM while for the two EC models the fire emission biases are caused by biases in normalized temperature and SPEI (Figure S3a). For the GFDL model, the overestimations over southeastern US are mostly attributed to the NN biases (Figure S3d).

4.3 Future fire emission projection

We use the NN model with the future climate and LAI from the eight GCMs, future population density from GPW, and present-day LULC from MODIS as predictors to project the future fire emissions in 2050-2065 under the SSP5-8.5 scenario and compare with the GCM-NN simulation driven with present-day GCM meteorology, GCM LAI, GPW population density, and MODIS LULC (i.e., land_fix experiment in Table 3). This method assumes stationarity of the relationships between fire emissions and their predictors learned by the NN model trained using observations. The projections only consider the effects of changes in meteorology, LAI, and population density and neglect the impacts of LULC changes. Figure 6 shows the spatial distributions of the ratio of future to present-day fire emissions. All GCM-NN models project increased fire emissions across the western US, with the largest enhancement over Pacific Northwest, northern California, and the southwestern US. For the southeastern US, five GCM-

NN models project decreased fire emissions in the future, while CMCC, GFDL, and CanESM project increased fire emissions.

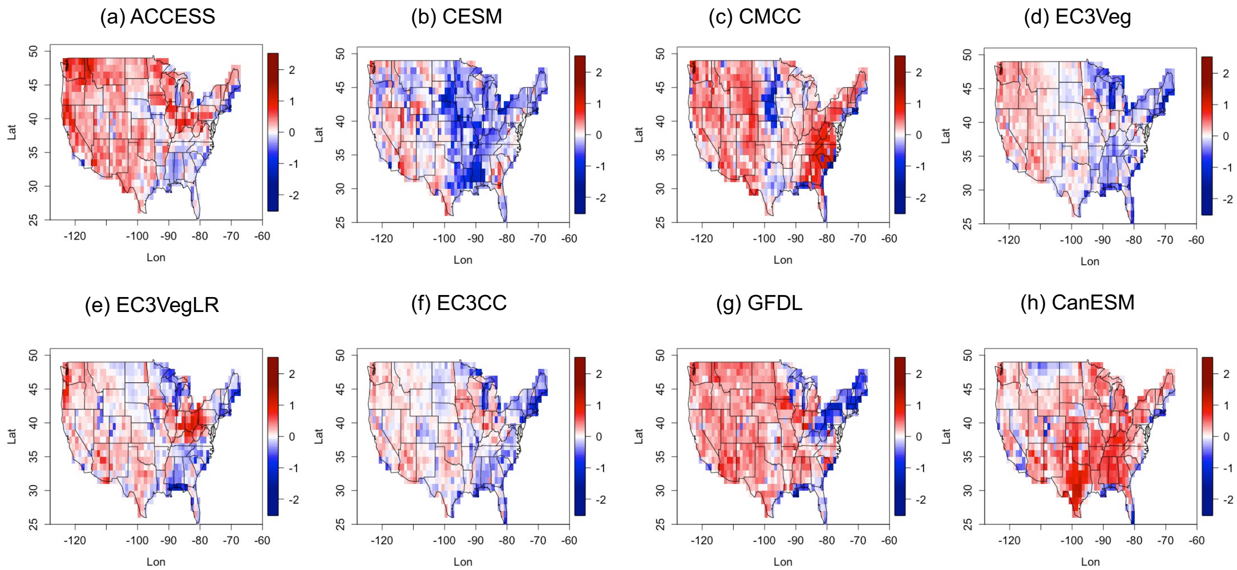

Fig. 6. Spatial distributions of the ratio of future (2050-2065) to present-day (2000-2014) fire $PM_{2.5}$ emissions. The ratio is shown in the base 10 logarithmic scale.

Over CONUS, the GCM-NN projects a median ratio of future to present-day fire emissions of 1.38, showing increased future fire emissions (Figure 7a). Across the four regions, the GCM-NN projects an increase in fire emissions of 13-115%, with the largest median ratio of 1.85 in the southwestern US (Figure 7a). Generally, more significant enhancement in fire emissions is found over the western US, where the western forest region and southern California have median ratios of 1.40 and 1.22, respectively. As for the southeastern US, different models project increases and decreases in fire emissions, resulting in a relatively small median ratio of 1.11. We further analyze the median ratios of future to present-day fire emissions for each region and season in Figure 7b. For CONUS, September-October-November (SON) and June-July-August (JJA) have the largest enhancement of fire emissions, with a median ratio of 1.7 and 1.58, respectively. Like CONUS, the western forest region is projected to have the largest enhancement of fire emissions in SON (median ratio = 2.29) and the second largest enhancement in JJA (median ratio = 1.67). For other regions, including southern California, southwestern US, and the southeastern US, the GCM-NN projects the greatest enhancement in JJA, with a median ratio of 1.82, 2.86, and 1.33, respectively (Figure 7b).

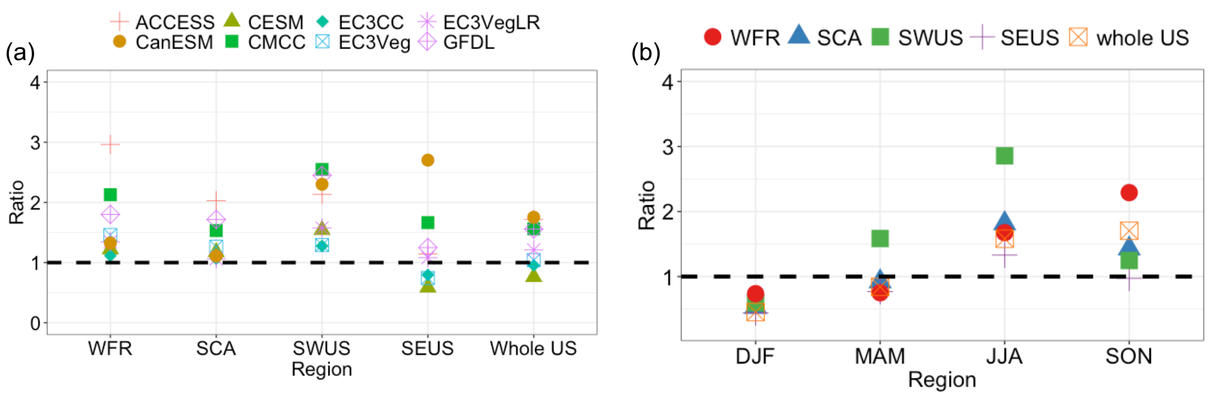

Fig. 7. (a) The ratio of future (2050-2065) to present-day (2000-2014) fire $PM_{2.5}$ emissions for CONUS and the four regions; (b) the median values of the ratios from 8 GCMs in CONUS and the four regions for each season.

Compared to the projections of fire carbon emissions by the GCMs (CESM2, EC3-Earth-CC, EC3-Earth-Veg, EC3-Earth-VegLR, and GFDL-ESM4.1) from CMIP6, the spatial patterns predicted by GCM-NN are very similar for present-day and future (Figure S4). Although the GCM-NN projection of $PM_{2.5}$ emissions is driven by the changes in meteorology, LAI, and population density, while the GCM projection of carbon emissions considers the changes in all factors including LULC changes, the predicted ratios of future to present-day fire emissions by the GCM-NN are within a similar range as the GCMs (Figures S5a and 5b). For the seasonality, since only CESM2 and GFDL-ESM1.4 provide monthly output, we compare the mean values of the two ratios for the four seasons over CONUS and the four regions. Both GCM and GCM-NN project the largest enhancement in JJA over CONUS (Figures S5c and 5d). However, there are differences in the peak seasons of enhancement for the four regions. For example, GCM-NN projects the largest enhancements of fire emissions in JJA, while GCM projects the largest enhancements in MAM for the western forest region and the southeastern US. The comparisons demonstrate the GCM-NN projections are generally consistent with the process-based models with DGVM embedded in GCMs despite the differences in the emitted species and peak fire seasons.

Lastly, we utilize the four GCM-NN models, which provides outputs of future vegetation distribution and LULC (GFDL-ESM4, EC-Earth3-CC, EC-Earth3-Veg, EC-Earth3-Veg-LR), to project fire emissions considering the effects of land use and land cover change in 2050-2065. These GCM-NN results (land_change) are compared with those predicted using the same LULC derived from MODIS for both the future and the present-day (land_fix) (Table 3). Figure 8a shows the median ratio of future to present-day fire emissions for CONUS and four regions based on the four GCMs. The projected median ratios increase for CONUS and the western US (WRF, SCA, and SWUS) by 58-83% when LULC changes are considered, which may be attributed to increases in vegetation, tree, and grass fraction in the future (Figure 8b) and these three land types are the predictors with larger contributions to the fire emissions (Figure 2). Note that vegetation fraction is the sum of tree, grass, shrub, and crop fraction. The results indicate the importance of land use and land cover in controlling future fire emissions. Meanwhile, large uncertainties exist in the projected land use and land cover change (Prestele et al., 2016).

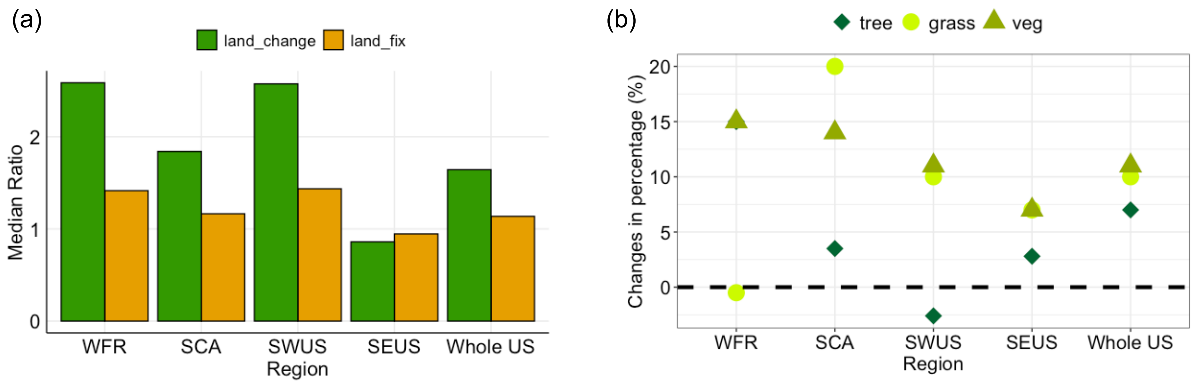

Fig. 8. (a) The median values of the ratio of future to present-day fire emissions from the four GCM-NN for CONUS and the four regions with and without including land use and land cover changes; (b) the percentage change of tree, grass, and vegetation fraction calculated as the differences in the average of the four models between 2050-2065 and 2000-2014 divided by the average of the four models over 2000-2014.

4.4 Factors driving increased fire emissions in the future

Figure 9 shows the differences in seasonal mean SHAP values between 2050-2065 and 2000-2014 from the eight GCM-NN for the four regions based on the projection excluding effects of future LULC changes (land_fix experiment). The SHAP values represent the contributions of the predictors, and the positive difference in SHAP values indicates increasing contribution to the future fire emissions. We show the changes in SHAP values for the summer (JJA) and fall (SON), as the larger enhancement of fire emissions is projected to occur in the two seasons for all the regions. For the western forest region, the increased fire emissions in JJA are driven by increasing normalized temperature and LAI and decreasing normalized RH and soil moisture (Figure 9a and Figure S6a). All of the GCMs show increased normalized temperature and LAI over the western forest region, with a median change of 29% and 20%, while the normalized RH and soil moisture only slightly decrease by 2.19% and 0.39% (Figure S6). Similar to the western forest region, the growing fire emissions in JJA in Southern California result from increasing normalized temperature and decreasing soil moisture, with a median change of 29% and -1.8%, respectively (Figure 9b and Figure S6b). For the southwestern US, decreased normalized RH (-4.6%) and soil moisture (-2.6%) as well as increased normalized temperature (+24%) and VPD (+18%) contribute to the enhanced fire emissions in summer (Figure 9c and Figure S6c). Lastly, increased normalized temperature and decreased normalized RH are the drivers of the increased fire emissions in JJA for the southeastern US (Figure 9d and Figure S6d). In the mid-21st century, normalized temperature is projected to increase by 23% and normalized RH is projected to decrease by 13% in JJA over the southeastern US. Interestingly, the changes in VPD contribution to fire emissions are much smaller than the changes in normalized temperature for the western US (Figures 9a-c). This can be explained by the fact that the increase in future VPD over western US is mainly driven by increasing temperature (Figures S6 and S7), so the NN model shows larger contributions from normalized temperature (Figure 2 and Figure 9).

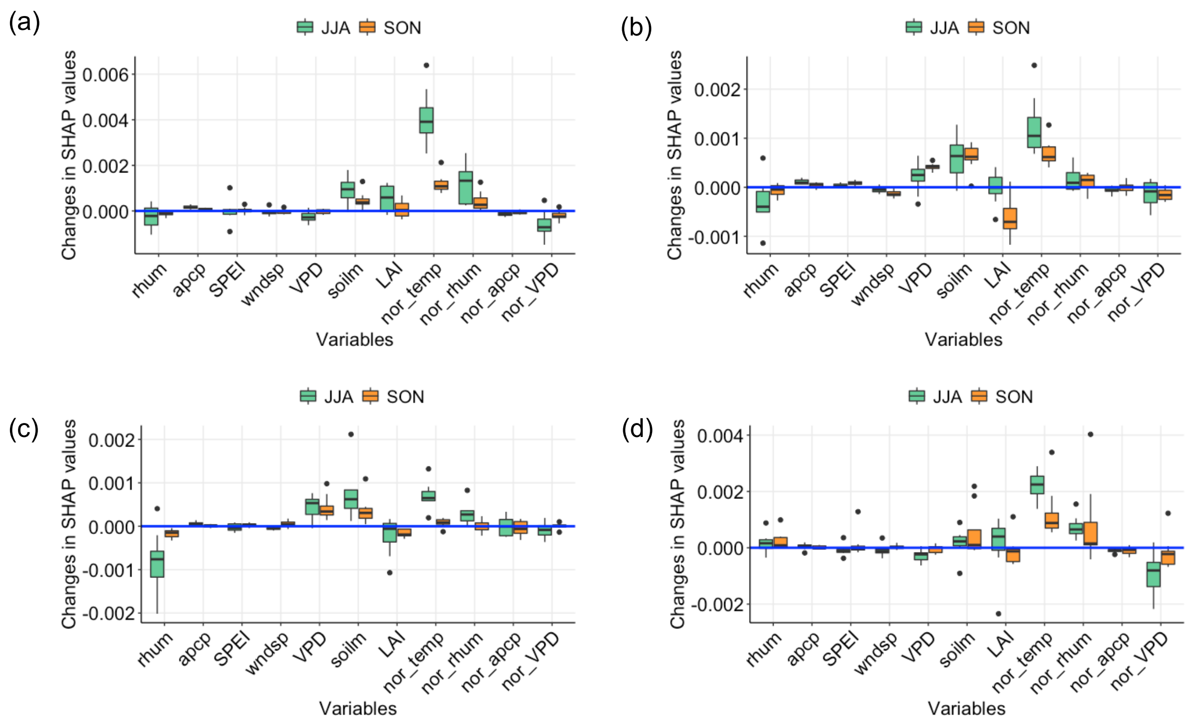

Fig. 9. The distributions of the changes in seasonal mean SHAP values from the eight GCMs between 2050-2065 and 2000-2014 for JJA and SON for the (a) western forest region, (b) Southern California, (c) southwestern US, and (d) southeastern US.

SON also shows larger fire emissions in the future, particularly over the western forest region and southern California, which are mainly contributed by increased normalized temperature and decreased soil moisture (Figures 9a and 9b). Normalized temperature is projected to increase by 336% and 164% in SON for the western forest region and southern California, respectively (Figure S8). The soil moisture in the two regions is projected to decrease by 3.2%. In summary, reduced soil moisture is the key common factor driving the increased fire emissions in both summer and fall across the western US (the western forest region, Southern California, and the southwestern US). Normalized temperature here represents the temporal variation of temperature. When we look at the actual changes in temperature across the 8 GCMs, the median temperature is projected to increase by 2.25~3.23 K in JJA and 2.60~2.80 K in SON for the four regions.

5 Discussions and conclusions

This study constructs a NN model explained by the SHAP to predict fire emissions and to understand factors driving the changes in fire emissions over CONUS in the mid-21st century under a high greenhouse gas emissions scenario (SSP5-8.5). The NN model shows promising results, with an RMSE of 0.085 g/m^2 and an IoA of 0.53 at 1° grid level, and it reproduces the interannual variability of the fire emissions over CONUS and selected regions (IoA=0.31-0.95). Although the NN model performance slightly degrades compared to the XGBoost model developed in Wang et al. (2022) due to coarser resolution and differences in the ML approaches, the NN model still outperforms other process-based models in simulating the spatial distribution and temporal variability of fire emissions. This study uses NN instead of XGBoost because the XGBoost cannot discriminate between the present-day and future meteorology simulated by the GCMs as both of their probability distributions fall within the probability distributions of the observations used for training, so the samples from the two periods would fall into the same node. On the other hand, NN can reflect the small changes in the inputs through the combination of weights and activation function.

Driven by the GCM outputs (i.e., GCM-NN) for the present-day, the GCM-NN predictions generally reproduce the observed seasonality of fire emissions, but the predicted spatial distributions of GCM-NN deviate from the GFED fire emissions. When we consider the contributions from NN biases and predictor biases, for ACCESS, CESM2, and CMCC, the overestimation of fire emissions over the Central Great Plains can be attributed to the NN biases. The overestimation in western forest region is due to biases in precipitation for CanESM and biases in normalized temperature and SPEI for the EC-Earth models, consistent with the warm and dry biases identified in the GCMs in CMIP6 (J. Dong et al., 2022; Srivastava et al., 2020). The positive biases over the southeastern US in GFDL-ESM can be mainly attributed to the NN biases.

The GCM-NN models project that fire emissions will increase by 38% (median value) in the mid-century under the SSP5-8.5 scenario, with a larger increase over the southwestern US (85%; median value) and western forest region (40%; median value). The largest enhancements are projected to occur in JJA for most selected regions, including southern California, southwestern US, and the southeastern US, with increases of 33-186%. As for the western forest region, fire emissions are projected to increase most in SON (129%). The projected increasing trends are consistent with the projections from prior studies (Table 1). For instance, Xie et al. (2022) showed that the fire CO_2 emissions are projected to increase by 130 to 260% over western North America under the SSP5-8.5 scenario using three CMIP6 earth system models. Although the emission species are different, our GCM-NN projects smaller increases in fire $PM_{2.5}$ emissions in summer over the western US (33-186%), as the GCM-NN does not consider the changes in LULC as well as the feedback between fire and climate. More recently, Liu et al. (2021) showed that the fire $PM_{2.5}$ emissions over the western US are projected to increase by 50% in the mid-21st century under the RCP8.5 scenario, which is close to the median value of the enhancement over the western US by our GCM-NN (~50%). Their projection considering future changes in fuel is roughly equal to the GCM-NN projection while our GCM-NN projection does not include future changes in fuel load. The smaller projected enhancements considering the changes in fuels may be due to fire model biases and smaller projected fuel changes (Liu et al., 2021). Considering the LULC change simulated by the four GCM models, the projected fire emissions by GCM-NN increase by 58-83% over the western US, compared to the future projection without LULC change. The projection considering future LULC change is close to the projection estimated by Xie et al. (2022), while the projected LULC change contains certain uncertainties (Prestele et al., 2016). Recent studies suggest that the climate sensitivity is substantially higher in CMIP6 than in CMIP5, showing more than one-quarter of models projecting warming larger than 4.7°C when doubling atmospheric CO_2 concentrations from pre-industrial levels (Ribes et al., 2021; Zelinka et al., 2020). The eight GCMs used in this study except for GFDL-ESM have higher equilibrium climate sensitivity (ECS) larger than the multimodel mean shown in Zelinka et al. (2020). Therefore, our projection using CMIP6 climate output may be subject to the "hotter" CMIP6 projection, but we focus on the median value of the multimodel projections, which would not be influenced by extreme values (i.e., the model with very high sensitivity).

Using SHAP to explain the NN model, we identify the crucial factors driving the future enhanced fire emissions over CONUS. Increased normalized temperature and decreased soil moisture and normalized RH are the common and key drivers leading to the enhanced fire emissions in JJA and SON across the western US (Figure 9). Soil moisture and RH is projected to decrease by 0.36-2.6% and 2.2-4.6%, respectively; the normalized temperature is projected to increase by 24-366% in the future, which is consistent with prior studies showing decreases in moisture and increases temperature will enhance future fire risk given abundant fuels (Jain et al., 2022). As shown in Figure 8, increases in fire emissions considering future LULC change may be attributed to increases in the grass, tree, and vegetation fraction (~15% across the western US). The fire emission projection generally agrees with the projections in prior studies and reveals the importance of the drying trend and LULC change in controlling future fire emissions (Brey et al., 2018; Yu et al., 2022).

This study utilizes XAI and CMIP6 GCM outputs to project future fire $PM_{2.5}$ emissions. This approach assumes the relationships between predictors and fire emissions remain the same in the future as at present, while the relationships may change. Uncertainties may exist in NN's extrapolation ability and behavior, which would be a concern for making future projections. For instance, prior studies have shown that the NN's structure and activation function and whether the training data is diverse have substantial impacts on extrapolation behavior (Xu et al., 2021). Hernanz et al. (2022) evaluated different MLs' extrapolation behavior in predicting surface temperature. Their results show that the extrapolation capability is better when training and testing data overlap at a certain level. In this study, the data space of the observation/reanalysis data and historical and future simulation of GCMs overlaps, suggesting minor extrapolated errors in our NN model projection (Figure S9). One notable limitation of the NN model is its lack of feedback between fire emissions and climate, which might underestimate the projection of future fire emissions (Zou et al., 2020). Lastly, large uncertainties also exist in the projection of future LULC; future work is needed to improve the future projection of LULC to better project fire emissions, as climate change projection can also be influenced by LULC change (Bukovsky et al., 2021). Overall, based on the relationships at present-day learned by NN, rising temperature, decreasing moisture, and changes in LULC (i.e., increases in vegetation) are key factors contributing to increasing future fire emissions over the western US, where the intensity and frequency of large fires have significantly risen in recent decades.

Acknowledgments

This research was supported by the U.S. Department of Energy Office of Science Biological and Environmental Research through the Regional and Global Model Analysis and Multisector Dynamics program areas. PNNL is operated by Battelle Memorial Institute for the U.S. Department of Energy under contract DE-AC06-76RLO-1830. This research was performed at PNNL and also partially funded under Assistance Agreement No. RD835871 by the U.S. Environmental Protection Agency to Yale University through the SEARCH (Solutions for Energy, AiR, Climate, and Health) Center. It has not been formally reviewed by EPA. The views expressed in this document are solely those of the SEARCH Center and do not necessarily reflect those of the Agency. EPA does not endorse any products or commercial services mentioned in this publication.

Open Research

The datasets and model output are publicly accessible online at

https://zenodo.org/record/7094709#.Yyj5y-zMLlw.

References

Abatzoglou, J. T. (2013). Development of gridded surface meteorological data for ecological applications and modelling. *International Journal of Climatology*, *33*(1), 121–131. https://doi.org/10.1002/joc.3413

Abatzoglou, J. T., & Kolden, C. A. (2013). Relationships between climate and macroscale area burned in the western United States. *International Journal of Wildland Fire*, *22*(7), 1003–1020. https://doi.org/10.1071/WF13019

Abatzoglou, J. T., & Williams, A. P. (2016). Impact of anthropogenic climate change on wildfire across western US forests. *Proceedings of the National Academy of Sciences*, *113*(42), 11770–11775. https://doi.org/10.1073/pnas.1607171113

Adadi, A., & Berrada, M. (2018). Peeking Inside the Black-Box: A Survey on Explainable Artificial Intelligence (XAI). *IEEE Access*, *6*, 52138–52160. https://doi.org/10.1109/ACCESS.2018.2870052

Akagi, S. K., Yokelson, R. J., Wiedinmyer, C., Alvarado, M. J., Reid, J. S., Karl, T., et al. (2011). Emission factors for open and domestic biomass burning for use in atmospheric models. *Atmospheric Chemistry and Physics*, *11*(9), 4039–4072. https://doi.org/10.5194/acp-11-4039-2011

Arrieta, A. B., Díaz-Rodríguez, N., Del Ser, J., Bennetot, A., Tabik, S., Barbado, A., et al. (2020). Explainable Artificial Intelligence (XAI): Concepts, taxonomies, opportunities and challenges toward responsible AI. *Information Fusion*, *58*, 82–115. https://doi.org/10.1016/j.inffus.2019.12.012

Birch, D. S., Morgan, P., Kolden, C. A., Abatzoglou, J. T., Dillon, G. K., Hudak, A. T., & Smith, A. M. S. (2015). Vegetation, topography and daily weather influenced burn severity in central Idaho and western Montana forests. *Ecosphere*, *6*(1), art17. https://doi.org/10.1890/ES14-00213.1

Brey, S. J., Barnes, E. A., Pierce, J. R., Wiedinmyer, C., & Fischer, E. V. (2018). Environmental Conditions, Ignition Type, and Air Quality Impacts of Wildfires in the Southeastern and Western United States. *Earth's Future*, *6*(10), 1442–1456. https://doi.org/10.1029/2018EF000972

Bukovsky, M. S., Gao, J., Mearns, L. O., & O'Neill, B. C. (2021). SSP-Based Land-Use Change Scenarios: A Critical Uncertainty in Future Regional Climate Change Projections. *Earth's Future*, *9*(3), e2020EF001782. https://doi.org/10.1029/2020EF001782

Burke, M., Driscoll, A., Heft-Neal, S., Xue, J., Burney, J., & Wara, M. (2021). The changing risk and burden of wildfire in the United States. *Proceedings of the National Academy of Sciences*, *118*(2). https://doi.org/10.1073/pnas.2011048118

CIESIN-Columbia University. (2017). Gridded Population of the World, Version 4 (GPWv4): Population Density, Revision 11 [Data set]. Palisades, NY: Socioeconomic Data and Applications Center (SEDAC). https://doi.org/10.7927/H49C6VHW

Coffield, S. R., Graff, C. A., Chen, Y., Smyth, P., Foufoula-Georgiou, E., & Randerson, J. T. (2019). Machine learning to predict final fire size at the time of ignition. *International Journal of Wildland Fire*, *28*, 861–873.

Cortez, P., & Morais, A. (2007). A Data Mining Approach to Predict Forest Fires using Meteorological Data (pp. 512–523). Portugal.

Crimmins, M. A. (2006). Synoptic climatology of extreme fire-weather conditions across the southwest United States. *International Journal of Climatology*, *26*(8), 1001–1016. https://doi.org/10.1002/joc.1300

Dillon, G. K., Holden, Z. A., Morgan, P., Crimmins, M. A., Heyerdahl, E. K., & Luce, C. H. (2011). Both topography and climate affected forest and woodland burn severity in two regions of the western US, 1984 to 2006. *Ecosphere*, *2*(12), art130. https://doi.org/10.1890/ES11-00271.1

Dong, J., Lei, F., & Crow, W. T. (2022). Land transpiration-evaporation partitioning errors responsible for modeled summertime warm bias in the central United States. *Nature Communications*, *13*(1), 336. https://doi.org/10.1038/s41467-021-27938-6

Dong, L., Leung, L. R., Qian, Y., Zou, Y., Song, F., & Chen, X. (2021). Meteorological Environments Associated With California Wildfires and Their Potential Roles in Wildfire Changes During 1984–2017. *Journal of Geophysical Research: Atmospheres*, *126*(5), e2020JD033180. https://doi.org/10.1029/2020JD033180

Döscher, R., Acosta, M., Alessandri, A., Anthoni, P., Arsouze, T., Bergman, T., et al. (2022). The EC-Earth3 Earth system model for the Coupled Model Intercomparison Project 6. *Geoscientific Model Development*, *15*(7), 2973–3020. https://doi.org/10.5194/gmd-15-2973-2022

Dunne, J. P., Horowitz, L. W., Adcroft, A. J., Ginoux, P., Held, I. M., John, J. G., et al. (2020). The GFDL Earth System Model Version 4.1 (GFDL-ESM 4.1): Overall Coupled Model Description and Simulation Characteristics. *Journal of Advances in Modeling Earth Systems*, *12*(11), e2019MS002015. https://doi.org/10.1029/2019MS002015

Eyring, V., Bony, S., Meehl, G. A., Senior, C. A., Stevens, B., Stouffer, R. J., & Taylor, K. E. (2016). Overview of the Coupled Model Intercomparison Project Phase 6 (CMIP6) experimental design and organization. *Geoscientific Model Development*, *9*(5), 1937–1958. https://doi.org/10.5194/gmd-9-1937-2016

Ford, B., Martin, M. V., Zelasky, S. E., Fischer, E. V., Anenberg, S. C., Heald, C. L., & Pierce, J. R. (2018). Future Fire Impacts on Smoke Concentrations, Visibility, and Health in the Contiguous United States. *GeoHealth*, *2*(8), 229–247. https://doi.org/10.1029/2018GH000144

Friedl, M., & Sulla-Menashe, D. (2015). MCD12C1 MODIS/Terra+Aqua Land Cover Type Yearly L3 Global 0.05Deg CMG V006 [Data set]. NASA EOSDIS Land Processes DAAC. https://doi.org/10.5067/MODIS/MCD12C1.006

Hernanz, A., García-Valero, J. A., Domínguez, M., & Rodríguez-Camino, E. (2022). A critical view on the suitability of machine learning techniques to downscale climate change projections: Illustration for temperature with a toy experiment. *Atmospheric Science Letters*, *23*(6), e1087. https://doi.org/10.1002/asl.1087

Hurtt, G. C., Chini, L., Sahajpal, R., Frolking, S., Bodirsky, B. L., Calvin, K., et al. (2020). Harmonization of global land use change and management for the period 850–2100 (LUH2) for CMIP6. *Geoscientific Model Development*, *13*(11), 5425–5464. https://doi.org/10.5194/gmd-13-5425-2020

IPCC. (2022). *Impacts, Adaptation, and Vulnerability. Contribution of Working Group II to the Sixth Assessment Report of the Intergovernmental Panel on Climate Change*. Cambridge University Press.

Jaffe, D. A., O'Neill, S. M., Larkin, N. K., Holder, A. L., Peterson, D. L., Halofsky, J. E., & Rappold, A. G. (2020). Wildfire and prescribed burning impacts on air quality in the United States. *Journal of the Air & Waste Management Association*, *70*(6), 583–615. https://doi.org/10.1080/10962247.2020.1749731

Jain, P., Castellanos-Acuna, D., Coogan, S. C. P., Abatzoglou, J. T., & Flannigan, M. D. (2022). Observed increases in extreme fire weather driven by atmospheric humidity and temperature. *Nature Climate Change*, *12*(1), 63–70. https://doi.org/10.1038/s41558-021-01224-1

Jones, B., & O'Neill, B. C. (2020). *Global One-Eighth Degree Population Base Year and Projection Grids Based on the Shared Socioeconomic Pathways*. Palisades, New York: NASA Socioeconomic Data and Applications Center (SEDAC). Retrieved from https://doi.org/10.7927/m30p-j498

Kane, V. R., Cansler, C. A., Povak, N. A., Kane, J. T., McGaughey, R. J., Lutz, J. A., et al. (2015). Mixed severity fire effects within the Rim fire: Relative importance of local climate, fire weather, topography, and forest structure. *Forest Ecology and Management*, *358*, 62–79. https://doi.org/10.1016/j.foreco.2015.09.001

Kaulfus, A. S., Nair, U., Jaffe, D., Christopher, S. A., & Goodrick, S. (2017). Biomass Burning Smoke Climatology of the United States: Implications for Particulate Matter Air Quality. *Environmental Science & Technology*, *51*(20), 11731–11741. https://doi.org/10.1021/acs.est.7b03292

Lawrence, D. M., Fisher, R. A., Koven, C. D., Oleson, K. W., Swenson, S. C., Bonan, G., et al. (2019). The Community Land Model Version 5: Description of New Features, Benchmarking, and Impact of Forcing Uncertainty. *Journal of Advances in Modeling Earth Systems*, *11*(12), 4245–4287. https://doi.org/10.1029/2018MS001583

Liu, Yawen, Zhang, K., Qian, Y., Wang, Y., Zou, Y., Song, Y., et al. (2018). Investigation of short-term effective radiative forcing of fire aerosols over North America using nudged hindcast ensembles. *Atmospheric Chemistry and Physics*, *18*(1), 31–47. https://doi.org/10.5194/acp-18-31-2018

Liu, Yongqiang, Liu, Y., Fu, J., Yang, C.-E., Dong, X., Tian, H., et al. (2021). Projection of future wildfire emissions in western USA under climate change: contributions from changes in wildfire, fuel loading and fuel moisture. *International Journal of Wildland Fire*, *31*(1), 1–13. https://doi.org/10.1071/WF20190

Lundberg, S., & Lee, S. (2017). A Unified Approach to Interpreting Model Predictions. Long Beach, CA, USA.

Marlon, J. R., Bartlein, P. J., Gavin, D. G., Long, C. J., Anderson, R. S., Briles, C. E., et al. (2012). Long-term perspective on wildfires in the western USA. *Proceedings of the National Academy of Sciences*, *109*(9), E535–E543. https://doi.org/10.1073/pnas.1112839109

McKinnon, K. A., Poppick, A., & Simpson, I. R. (2021). Hot extremes have become drier in the United States Southwest. *Nature Climate Change*, *11*(7), 598–604. https://doi.org/10.1038/s41558-021-01076-9

Mesinger, F., DiMego, G., Kalnay, E., Mitchell, K., Shafran, P. C., Ebisuzaki, W., et al. (2006). North American Regional Reanalysis. *Bulletin of the American Meteorological Society*, *87*(3), 343–360. https://doi.org/10.1175/BAMS-87-3-343

Myneni, R., Knyazikhin, Y., & Park, T. (2015). MCD15A2H MODIS/Terra+Aqua Leaf Area Index/FPAR 8-day L4 Global 500m SIN Grid V0006. *NASA EOSDIS Land Processes DAAC*. https://doi.org/10.5067/MODIS/MCD15A2H.006

Neumann, J. E., Amend, M., Anenberg, S., Kinney, P. L., Sarofim, M., Martinich, J., et al. (2021). Estimating PM2.5-related premature mortality and morbidity associated with future wildfire emissions in the western US. *Environmental Research Letters*, *16*(3), 035019. https://doi.org/10.1088/1748-9326/abe82b

NIFC. (2022). *Suppression Costs*. National Interagency Fire Center. Retrieved from https://www.nifc.gov/fire-information/statistics/suppression-costs

O'Dell, K., Ford, B., Fischer, E. V., & Pierce, J. R. (2019). Contribution of Wildland-Fire Smoke to US PM2.5 and Its Influence on Recent Trends. *Environmental Science & Technology*, *53*(4), 1797–1804. https://doi.org/10.1021/acs.est.8b05430

O'Neill, B. C., Tebaldi, C., van Vuuren, D. P., Eyring, V., Friedlingstein, P., Hurtt, G., et al. (2016). The Scenario Model Intercomparison Project (ScenarioMIP) for CMIP6. *Geoscientific Model Development*, *9*(9), 3461–3482. https://doi.org/10.5194/gmd-9-3461-2016

Padarian, J., McBratney, A. B., & Minasny, B. (2020). Game theory interpretation of digital soil mapping convolutional neural networks. *SOIL*, *6*(2), 389–397. https://doi.org/10.5194/soil-6-389-2020

Pechony, O., & Shindell, D. T. (2009). Fire parameterization on a global scale. *Journal of Geophysical Research: Atmospheres*, *114*(D16). https://doi.org/10.1029/2009JD011927

Prestele, R., Alexander, P., Rounsevell, M. D. A., Arneth, A., Calvin, K., Doelman, J., et al. (2016). Hotspots of uncertainty in land-use and land-cover change projections: a global-scale model comparison. *Global Change Biology*, *22*(12), 3967–3983. https://doi.org/10.1111/gcb.13337

Ribes, A., Qasmi, S., & Gillett, N. P. (2021). Making climate projections conditional on historical observations. *Science Advances*, *7*(4), eabc0671. https://doi.org/10.1126/sciadv.abc0671

Shankar, U., Prestemon, J. P., McKenzie, D., Talgo, K., Xiu, A., Omary, M., et al. (2018). Projecting wildfire emissions over the south-eastern United States to mid-century. *International Journal of Wildland Fire*, *27*(5), 313–328. https://doi.org/10.1071/WF17116

Song, X., Wang, D.-Y., Li, F., & Zeng, X.-D. (2021). Evaluating the performance of CMIP6 Earth system models in simulating global vegetation structure and distribution. *Advances in Climate Change Research*, *12*(4), 584–595. https://doi.org/10.1016/j.accre.2021.06.008

Srivastava, A., Grotjahn, R., & Ullrich, P. A. (2020). Evaluation of historical CMIP6 model simulations of extreme precipitation over contiguous US regions. *Weather and Climate Extremes*, *29*, 100268. https://doi.org/10.1016/j.wace.2020.100268

Stirnberg, R., Cermak, J., Kotthaus, S., Haeffelin, M., Andersen, H., Fuchs, J., et al. (2021). Meteorology-driven variability of air pollution (PM_1) revealed with explainable machine learning. *Atmospheric Chemistry and Physics*, *21*(5), 3919–3948. https://doi.org/10.5194/acp-21-3919-2021

Swart, N. C., Cole, J. N. S., Kharin, V. V., Lazare, M., Scinocca, J. F., Gillett, N. P., et al. (2019). The Canadian Earth System Model version 5 (CanESM5.0.3). *Geoscientific Model Development*, *12*(11), 4823–4873. https://doi.org/10.5194/gmd-12-4823-2019

Thonicke, K., Spessa, A., Prentice, I. C., Harrison, S. P., Dong, L., & Carmona-Moreno, C. (2010). The influence of vegetation, fire spread and fire behaviour on biomass burning and trace gas emissions: results from a process-based model. *Biogeosciences*, *7*(6), 1991–2011. https://doi.org/10.5194/bg-7-1991-2010

Trouet, V., Taylor, A. H., Carleton, A. M., & Skinner, C. N. (2009). Interannual variations in fire weather, fire extent, and synoptic-scale circulation patterns in northern California and Oregon. *Theoretical and Applied Climatology 95: 349-360*, *95*, 349–360. https://doi.org/10.1007/s00704-008-0012-x

Val Martin, M., Heald, C. L., Lamarque, J.-F., Tilmes, S., Emmons, L. K., & Schichtel, B. A. (2015). How emissions, climate, and land use change will impact mid-century air quality over the United States: a focus on effects at national parks. *Atmospheric Chemistry and Physics*, *15*(5), 2805–2823. https://doi.org/10.5194/acp-15-2805-2015

Vicente-Serrano, S. M., Beguería, S., & López-Moreno, J. I. (2010). A Multiscalar Drought Index Sensitive to Global Warming: The Standardized Precipitation Evapotranspiration Index. *Journal of Climate*, *23*(7), 1696–1718. https://doi.org/10.1175/2009JCLI2909.1

Wang, S. S.-C., & Wang, Y. (2020). Quantifying the effects of environmental factors on wildfire burned area in the south central US using integrated machine learning techniques. *Atmospheric Chemistry and Physics*, *20*(18), 11065–11087. https://doi.org/10.5194/acp-20-11065-2020

Wang, S. S.-C., Qian, Y., Leung, L. R., & Zhang, Y. (2021). Identifying key drivers of wildfires in the contiguous US using machine learning and game theory interpretation. *Earth's Future*, *9*(6), e2020EF001910. https://doi.org/10.1029/2020EF001910

Wang, S. S.-C., Qian, Y., Leung, L. R., & Zhang, Y. (2022). Interpreting machine learning prediction of fire emissions and comparison with FireMIP process-based models. *Atmospheric Chemistry and Physics*, *22*(5), 3445–3468. https://doi.org/10.5194/acp-22-3445-2022 van der Werf, G. R., Randerson, J. T., Giglio, L., van Leeuwen, T. T., Chen, Y., Rogers, B. M., et al. (2017). Global fire emissions estimates during 1997–2016. *Earth System Science Data*, *9*(2), 697–720. https://doi.org/10.5194/essd-9-697-2017

Westerling, A. L., Hidalgo, H. G., Cayan, D. R., & Swetnam, T. W. (2006). Warming and Earlier Spring Increase Western U.S. Forest Wildfire Activity. *Science*, *313*(5789), 940–943. https://doi.org/10.1126/science.1128834

Xia, Y., Mitchell, K., Ek, M., Sheffield, J., Cosgrove, B., Wood, E., et al. (2012). Continental-scale water and energy flux analysis and validation for the North American Land Data Assimilation System project phase 2 (NLDAS-2): 1. Intercomparison and application of model products. *Journal of Geophysical Research: Atmospheres*, *117*(D3). https://doi.org/10.1029/2011JD016048

Xie, Y., Lin, M., Decharme, B., Delire, C., Horowitz, L. W., Lawrence, D. M., et al. (2022). Tripling of western US particulate pollution from wildfires in a warming climate. *Proceedings of the National Academy of Sciences*, *119*(14), e2111372119. https://doi.org/10.1073/pnas.2111372119

Xu, K., Zhang, M., Li, J., Du, S. S., Kawarabayashi, K., & Jegelka, S. (2021, March 2). How Neural Networks Extrapolate: From Feedforward to Graph Neural Networks. arXiv. https://doi.org/10.48550/arXiv.2009.11848

Yu, Y., Mao, J., Wullschleger, S. D., Chen, A., Shi, X., Wang, Y., et al. (2022). Machine learning–based observation-constrained projections reveal elevated global socioeconomic risks from wildfire. *Nature Communications*, *13*(1), 1250. https://doi.org/10.1038/s41467-022-28853-0

Yue, X., Mickley, L. J., Logan, J. A., & Kaplan, J. O. (2013). Ensemble projections of wildfire activity and carbonaceous aerosol concentrations over the western United States in the mid-21st century. *Atmospheric Environment*, *77*, 767–780. https://doi.org/10.1016/j.atmosenv.2013.06.003

Zelinka, M. D., Myers, T. A., McCoy, D. T., Po-Chedley, S., Caldwell, P. M., Ceppi, P., et al. (2020). Causes of Higher Climate Sensitivity in CMIP6 Models. *Geophysical Research Letters*, *47*(1), e2019GL085782. https://doi.org/10.1029/2019GL085782

Zhong, S., Yu, L., Heilman, W. E., Bian, X., & Fromm, H. (2020). Synoptic weather patterns for large wildfires in the northwestern United States—a climatological analysis using three classification methods. *Theoretical and Applied Climatology*, *76*. https://doi.org/10.1007/s00704-020-03235-y

Zhu, Q., Li, F., Riley, W. J., Xu, L., Zhao, L., Yuan, K., et al. (2022). Building a machine learning surrogate model for wildfire activities within a global Earth system model. *Geoscientific Model Development*, *15*(5), 1899–1911. https://doi.org/10.5194/gmd-15-1899-2022

Ziehn, T., Chamberlain, M. A., Law, R. M., Lenton, A., Bodman, R. W., Dix, M., et al. (2020). The Australian Earth System Model: ACCESS-ESM1.5. *Journal of Southern Hemisphere Earth Systems Science*, *70*(1), 193–214. https://doi.org/10.1071/ES19035

Zou, Y., Wang, Y., Qian, Y., Tian, H., Yang, J., & Alvarado, E. (2020). Using CESM-RESFire to understand climate–fire–ecosystem interactions and the implications for decadal climate variability. *Atmospheric Chemistry and Physics*, *20*(2), 995–1020. https://doi.org/10.5194/acp-20-995-2020